Performance of Stand-alone Hybrid Wind-Photovoltaic System with Battery Storage

O. E. M. Youssef, N. M. B. Abdel-Rahim, A. Shaltout

Faculty of Engineering at Shoubra, Benha University, Cairo, Egypt

Faculty of Engineering, Cairo University, Giza, Egypt

omsamoh@yahoo.com nabdelrahim@gmail.com aashaltout@yahoo.com

Abstract- **Stand-alone systems using renewable energy sources, such as wind energy and photovoltaic (PV) energy with storage battery banks are commonly used to supply remote houses. Stand-alone hybrid wind-PV system with battery storage is considered in this paper. It is proposed to employ squirrel-cage induction generator (SCIG) in wind subsystem. Pulse-width modulation (PWM) rectifier is used to control the SCIG. The proposed control scheme employs the direct torque control (DTC) strategy to modulate the ON / OFF durations of the switching devices of the PWM rectifier to ensure maximum power extraction through the SCIG operation. Furthermore, the control scheme rids the proposed system from the need of dedicated external capacitors for exciting the SCIG. Instead, the required reactive power of the SCIG is provided by the switching of the PWM rectifier. Simulation results are provided in the paper to demonstrate the capabilities of the system.**

I. INTRODUCTION

Renewable energy sources, such as wind energy and photovoltaic (PV) energy, are used by stand-alone systems supplying remote houses. These sources are of intermittent nature and, therefore, the stand-alone systems should include storage battery banks. The storage battery banks improve the reliability of these systems because the excess energy is stored in the battery bank, and this energy is delivered to the load when the available energy is not sufficient.

Wind energy and photovoltaic energy have complementary characters. Combining wind energy and photovoltaic in one system (hybrid system) increases the reliability of this system and reduces the storage batteries [1]–[4].

The general configuration of stand-alone hybrid wind-PV system with battery storage is shown in Fig. 1, where the generator used by the wind subsystem is a permanent-magnet synchronous generator (PMSG) [1], [5], [6].

Compared to induction generator, PMSG is sensitive to heat and of high cost. However, stand-alone hybrid wind-PV system with battery storage using induction generator is not investigated in the literature.

In this paper, it is proposed to use squirrel-cage induction generator (SCIG) instead of PMSG, and to use direct torque control (DTC) technique in the wind subsystem. This controlled generator is used in collaboration with the PV unit to build the stand-alone hybrid system.

It is commonly known that there is a maximum voltage limit of the battery bank to protect the battery bank against overcharging [6]–[9]. Therefore, it is required to capture the maximum power from the renewable energy source provided that the maximum voltage limit is not exceeded [6]. The voltage constraint will be followed in this paper to determine the load sharing of the PV and wind energy subsystems.

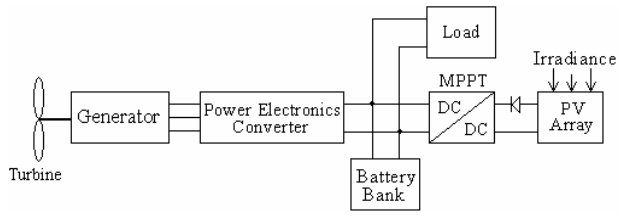

Fig. 1 General configuration of stand-alone hybrid wind-PV system.

II. CHARACTERISTICS OF PV ARRAY

The PV array consists of parallel-connected strings with each string consisting of a number of series-connected modules. Each PV module consists of series connected PV cells [10], [11]. The dependency of the current–voltage characteristics of the PV array on solar radiation (G) is shown in Fig. 2 [12].

III. MODELING OF BATTERY

The lead-acid batteries can be represented by the equivalent circuit shown in Fig. 3 [8], [13], [14].

where

R_c , R_d internal charge and discharge resistances

U_{bat} , U_{boc} battery terminal and open-circuit voltages

i_{bat} battery current

C_b battery capacitance

The battery bank has a maximum voltage limit for the protection against the overcharging [6]–[9].

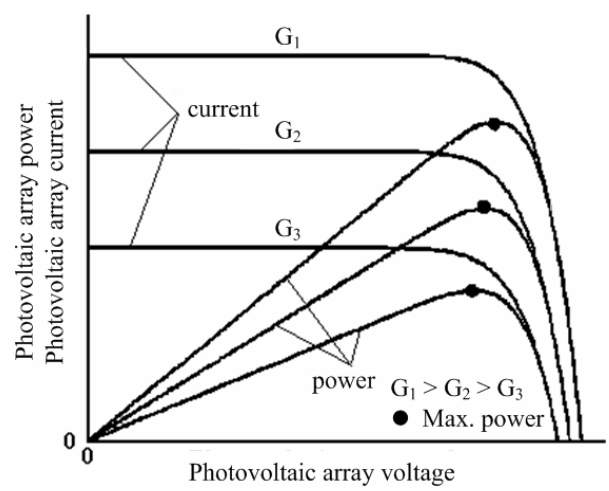

Fig. 2 PV array characteristics.

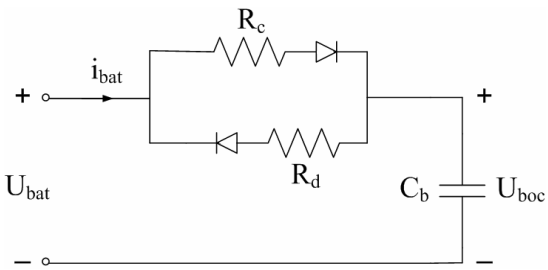

Fig. 3 Lead-cid battery equivalent circuit (directions of currents are during charging period).

IV. PV SUBSYSTEM CONTROL

A. Maximum Power-Point Tracking (MPPT)

There are different MPPT techniques to obtain maximum power operation of PV array. In this paper, direct maximum-power-point tracking (DMPPT) technique is used [15]. In this method, the duty ratio (D) of the DC-DC converter is controlled by directly using the output power of the PV array (P_g). The condition of maximum power point which is tracked by the control of the DC-DC converter is

$$\frac{dP_g}{dD} = 0 \tag{1}$$

The duty ratio is increased or decreased periodically, according to the values of ΔP_g and ΔD, to move the operating point toward the maximum power point.

B. Modes of PV Subsystem Control

As aforementioned, the battery-bank voltage must be taken in account to protect the battery bank against overcharging. According to the battery-bank voltage (u_{dc}), we have two modes of operation. Mode 1 is when $u_{dc} \le U_{max}$, and Mode 2 is when $u_{dc} > U_{max}$, where U_{max} is the maximum voltage limit of the battery bank. Fig. 4 illustrates these operating modes. When the voltage u_{dc} is increased beyond U_{max} , the relationship ($u_{dc} = U_{max}$) is maintained by decreasing the captured power. The captured power is decreased according to the values of ΔP_g and ΔD, to move the operating point away from the maximum power point.

V. CHARACTERISTICS OF WIND TURBINE

The developed mechanical power of a turbine rotor is given by [16]–[18]:

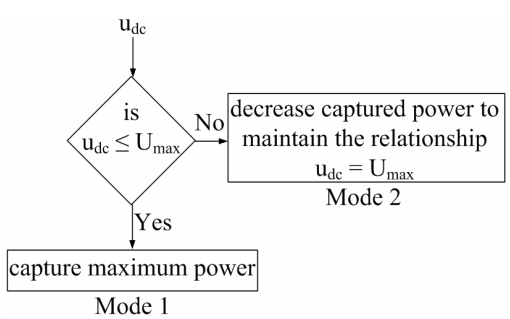

Fig. 4 Modes of operation of PV subsystem.

$$P_m = \frac{1}{2} C_p \rho A V_w^3 \tag{2}$$

where C_p is the power coefficient, ρ is the air density, V_w is the wind speed and A is the area swept by the wind turbine. The swept area is give by

$$A = \pi R^2 \tag{3}$$

where R is the radius of the turbine rotor.

The power coefficient is given as a function of tip-speed ratio (α). The relationship between α and C_P of a wind turbine is given in Fig. 5, where α is given by

$$\alpha = \frac{\text{tip speed of rotor blades}}{\text{wind speed}} = \frac{\omega R}{V_w} \tag{4}$$

where ω is the angular velocity of the turbine shaft.

Using (2) and (4), and for certain wind speeds, the mechanical power (P_m) can be plotted against the turbine speed as shown in Fig. 6. This figure shows that to maximize the extracted power, the rotor speed must be varied with wind speed.

Fig. 7 shows a typical power curve of a wind turbine. The design of the wind turbine is such that the generation is started at the cut-in wind speed ($V_{cut\text{-}in}$) . In the constant-maximum C_p region, the operation is at optimum value of α (α_{opt}). The output power is equal to its rated value from the rated speed (V_{rated}) to the cut-out speed ($V_{cut\text{-}out}$) [17], [19].

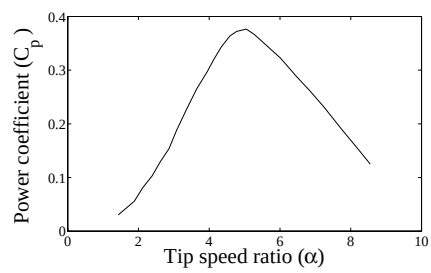

Fig. 5 Power coefficient (C_p) versus tip-speed ratio (α).

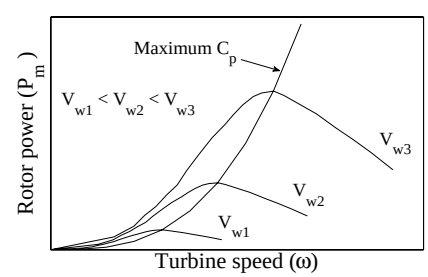

Fig. 6 Mechanical power against rotor speed for different wind speeds.

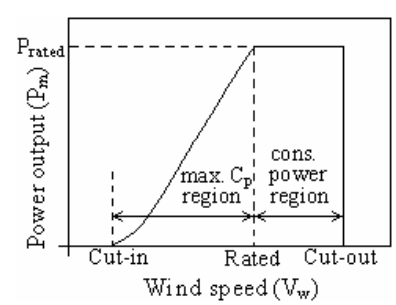

Fig. 7 Typical power curve of a wind turbine generator.

VI. WIND SUBSYSTEM CONTROL

A. Control Scheme of Wind Subsystem

The generator used by the wind subsystem is squirrel-cage induction generator (SCIG), and it is controlled by the direct torque control (DTC) technique. The reactive power required by SCIG is not obtained by using excitation capacitors. By using DTC technique, this reactive power is obtained from the battery bank by the switching pattern of the PWM rectifier. Also, DTC technique is used to capture the maximum power from the wind turbine, where this power must not exceed the rated power of the wind turbine, provided that the maximum voltage limit (U_{max}) of the battery bank is not exceeded. Details of control scheme are given in [20].

B. Modes of Wind Subsystem Control

According to the battery-bank voltage (u_{dc}), we have two modes of operation. Mode 1 is when $u_{dc} \leq U_{max}$, and Mode 2 is when $u_{dc} > U_{max}$. Fig. 8 illustrates these operating modes.

In Mode 1 of operation, the required operation of the system is according to the power curve of the wind turbine, Fig. 7, where it is required to capture the maximum power from cut-in to rated wind speeds, and to capture the rated power from rated to cut-out wind speeds. This mode is explained in Fig. 9. In Fig. 9(a) the wind speed is increased from V_{w1} to V_{w2} where $V_{w2} \leq V_{rated}$. The captured power follows the path X-Y-Z. In Fig. 9(b) the wind speed is increased from V_{w1} to V_{w2} where $V_{w2} > V_{rated}$. In Mode 2 of operation, the turbine is accelerated beyond ω_{opt} to operate at the power that makes u_{dc} equals U_{max} . This power is less than the captured power in Mode 1 for the same wind speed. This mode is explained by Fig. 10. The captured power follows the path X-Y-Z.

VII. OPERATION OF THE HYBRID SYSTEM

This section is devoted to examine the behavior of the hybrid system. Each of the two subsystems; namely PV subsystem and wind subsystem is controlled by its own controller. In Mode 1, each controller will guide its own system to track the maximum power. In Mode 2, the two controllers are coordinated to follow the maximum voltage constraint.

Data of the hybrid system is given in Appendix I. The system is simulated using MATLAB/SIMULINK [21]. To study Mode 1 of PV subsystem and wind subsystem, state of charge (SOC) of the battery bank is chosen of low value to operate at $u_{dc} < U_{max}$.

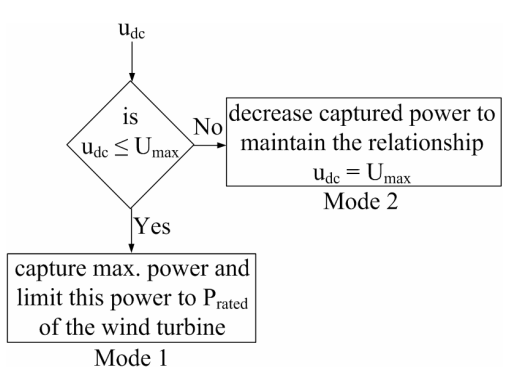

Fig. 8 Modes of operation of wind subsystem.

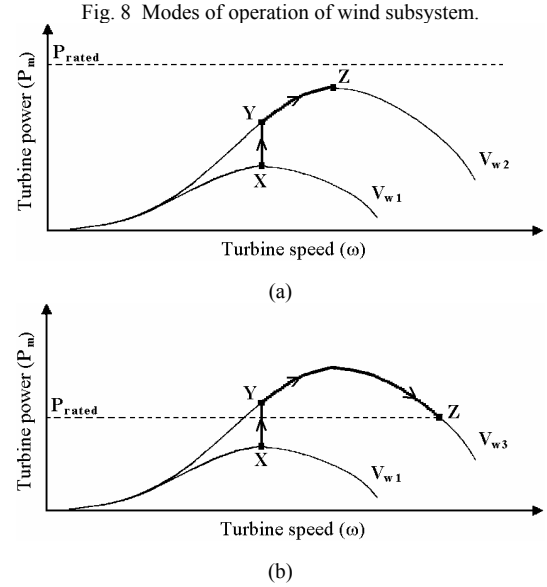

Fig. 9 Mode 1 of operation.

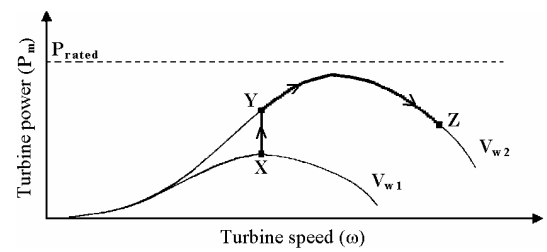

Fig. 10 Mode 2 of operation.

For Mode 1 and when $V_{w2} \leq V_{rated}$, results for SOC = 0.3, wind speed (V_w) changed suddenly from 4 m/s ($V_{cut\text{-}in}$) to 10.5 m/s (V_{rated}) at time equal to 1.5 s and insolation level (G) changed suddenly from 0.1kW/m^2 to 1kW/m^2 at time equal to 1.5 s are shown in Figs. 11 to 14. Fig. 11 shows that the steady-state captured power of PV array is about 1195.6 watt, while the rated power of PV array is about 1205 watt. Therefore, this captured power has about 0.78 % deviation, and good peak-power operation is obtained. Fig. 12 shows that the captured power from the wind turbine is increased gradually, starting from the time of change of wind speed, until maximum power operation is obtained. The steady-state captured power is about 986.7 watt, while the rated power of wind turbine is about 994 watt. Therefore, this captured power has about 0.73 % deviation, and good peak-power operation is obtained. Also, Fig. 12 shows that the turbine speed is increased gradually to the value corresponding to maximum power operation. The steady-state turbine speed is about (47.05 rad/s), while the optimal-turbine speed corresponding to optimal maximum power is about (48.09 rad/s). Therefore, this turbine speed has about 2.16 % deviation. Fig. 13 shows that the DC-bus voltage is less than its maximum value (U_{max}), where U_{max} is about 130.4 V, confirming Mode 1 of operation. Fig. 14 shows that the steady-state phase current of the induction generator is nearly sinusoidal current with total-harmonic distortion (THD) of about 8.79 %.

For Mode 1 and when $V_{w2} > V_{rated}$, results for SOC = 0.3, wind speed (V_w) changed suddenly from 10.5 m/s (V_{rated}) to 15 m/s at time equal to 1.5 s and insolation level (G) changed suddenly from 0.1kW/m^2 to 1kW/m^2 at time equal to 1.5 s are shown in Figs. 15 to 18. Fig. 15 shows that the steady-state captured power of PV array is about 1198 watt, while the rated power of PV array is about 1205 watt. Therefore, this captured power has about 0.58 % deviation, and good peak-power operation is obtained. Fig. 16 shows that the captured power from the wind turbine is increased beyond rated power of the turbine, starting from the time of change of wind speed, until rated power operation is obtained. Also, Fig. 16 shows that the turbine speed is increased gradually to turbine speed corresponding to rated power operation. The steady-state turbine speed is about 1095 rpm (114.7 rad/s), while the required turbine speed corresponding to rated power operation is about 1107 rpm (115.9 rad/s). Therefore, the turbine speed has about 1.1 % deviation. Fig. 17 shows that the DC-bus voltage is less than its maximum value (U_{max}), where U_{max} is about 130.4 V, confirming Mode 1 of operation. Fig. 18 shows that the steady-state phase current of the induction generator is nearly sinusoidal current with total-harmonic distortion (THD) of about 8.4 %.

To study Mode 2 of PV subsystem and wind subsystem, SOC of the battery bank is chosen of high value to make the value of u_{dc} increases to U_{max} . Results for SOC = 0.9, wind speed (V_w) changed suddenly from 4 m/s ($V_{cut\text{-}in}$) to 10.5 m/s (V_{rated}) at time equal 1.5 s are shown in Figs. 19 to 22. Fig. 19 shows that the steady-state captured power of the PV array is reduced to a value that makes u_{dc} equal to U_{max} . Fig. 20 shows that the captured power from the wind turbine is increased gradually, starting from the time of change of wind speed, and crossing its maximum value. Finally, the captured power from the wind turbine is at a value that makes u_{dc} equal to U_{max} . Also, Fig. 19 shows that the turbine speed is increased gradually to turbine speed corresponding to the power operation that makes u_{dc} equal to U_{max} . Fig. 21 shows the DC-bus voltage with steady-state mean value of about 130.28 V, while the maximum DC-bus voltage is about 130.4 V. Therefore, the mean DC-bus voltage has about 0.084 % deviation, and good maximum voltage operation is obtained. Fig. 22 shows the steady-state phase current of the induction generator. The distortion in the phase current is due to the control reaction of the wind subsystem against the increasing of the battery-bank voltage (u_{dc}) beyond the maximum value. During the acceleration of the generator and turbine, there is no increasing in the voltage u_{dc} corresponding to the rising of the turbine power (P_m) because this power is stored as kinetic energy in the rotating parts.

It should be noted that the voltage u_{dc} reaches its maximum voltage limit (U_{max}) although the battery bank is not fully charged. This is due to the internal resistance of the battery bank. However, SOC will increase gradually to full-charge state.

The reduction of captured power shown in Figs. 19 and 20 will decrease if the system supplies higher loads. To explain this condition, Figs. 23 and 24 show the captured power when a load of R_L of 20 Ω is connected to the DC-bus. It is clear that the total captured power is increased due to the load connection.

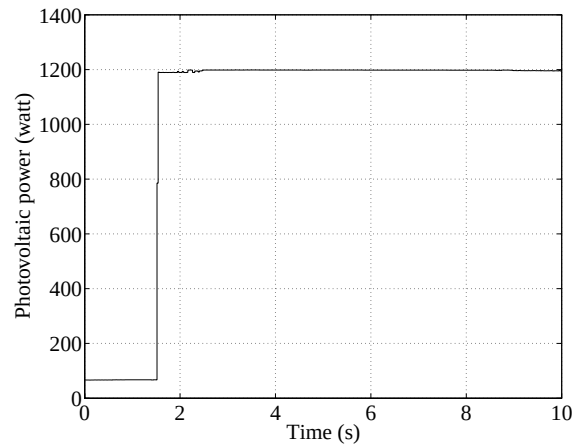

Fig. 11 Captured power of PV array for SOC = 0.3, G changed suddenly from 0.1 kW/m^2 to 1 kW/m^2 at t = 1.5 s and V_w changed suddenly from 4 m/s to 10.5 m/s at t = 1.5 s.

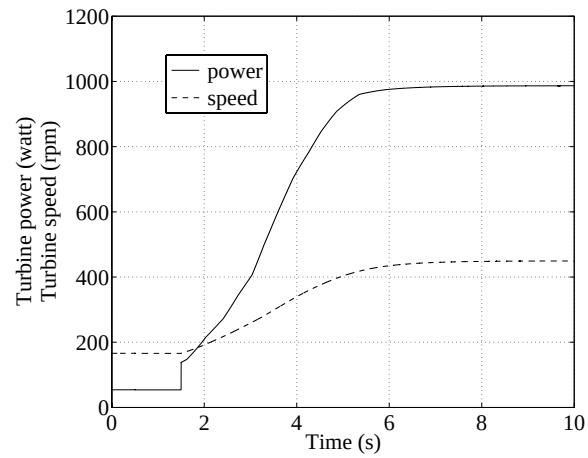

Fig. 12 Captured power of wind turbine and turbine speed for SOC = 0.3, G changed suddenly from 0.1 kW/m^2 to 1 kW/m^2 at t = 1.5 s and V_w changed suddenly from 4 m/s to 10.5 m/s at t = 1.5 s.

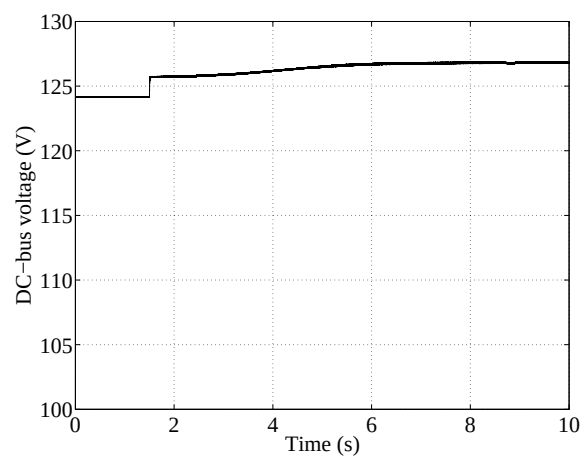

Fig. 13 DC-bus voltage for SOC = 0.3, G changed suddenly from 0.1 kW/m^2 to 1 kW/m^2 at t = 1.5 s and V_w changed suddenly from 4 m/s to 10.5 m/s at t = 1.5 s.

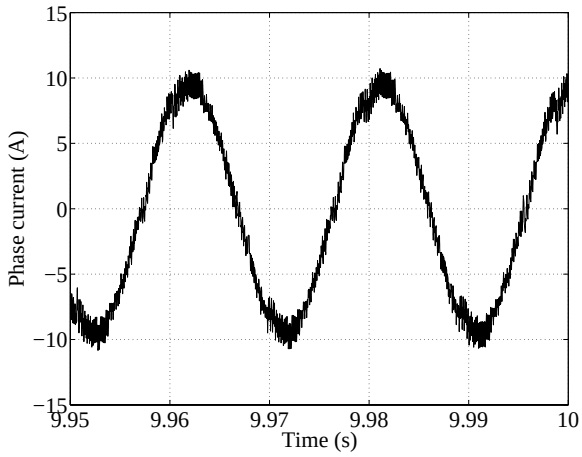

Fig. 14 Steady-state phase current of the induction generator for no load, SOC = 0.3, G changed suddenly from 0.1 kW/m^2 to 1 kW/m^2 at t = 1.5 s and V_w changed suddenly from 4 m/s to 10.5 m/s at t = 1.5 s.

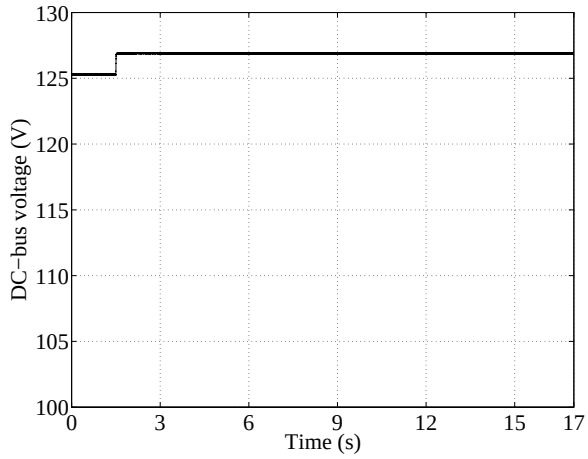

Fig. 17 DC-bus voltage for SOC = 0.3, G changed suddenly from 0.1 kW/m^2 to 1 kW/m^2 at t = 1.5 s and V_w changed suddenly from 10.5 m/s to 15 m/s at t = 1.5 s.

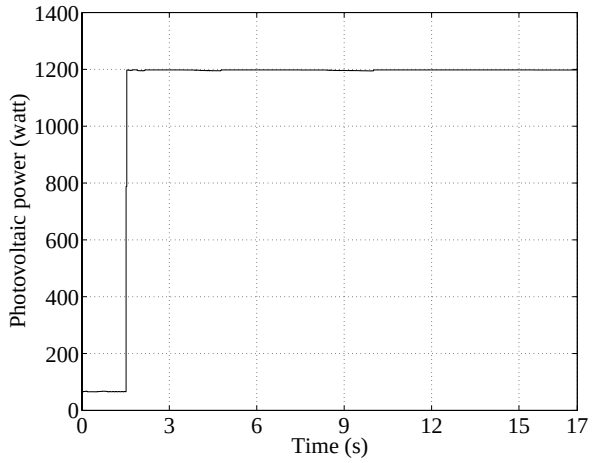

Fig. 15 Captured power of PV array for SOC = 0.3, G changed suddenly from 0.1 kW/m^2 to 1 kW/m^2 at t = 1.5 s and V_w changed suddenly from 10.5 m/s to 15 m/s at t = 1.5 s.

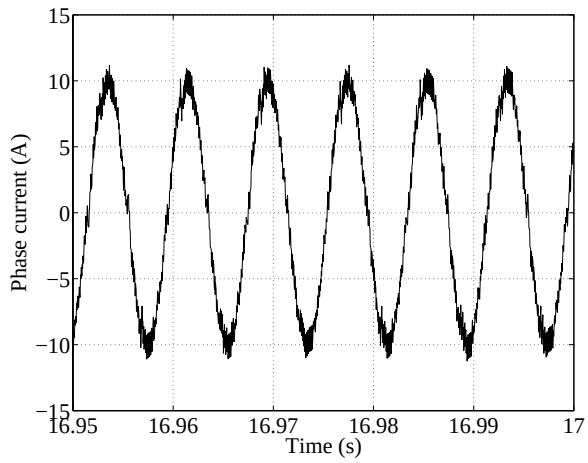

Fig. 18 Steady-state phase current for SOC = 0.3, G changed suddenly from 0.1 kW/m^2 to 1 kW/m^2 at t = 1.5 s and V_w changed suddenly from 10.5 m/s to 15 m/s at t = 1.5 s.

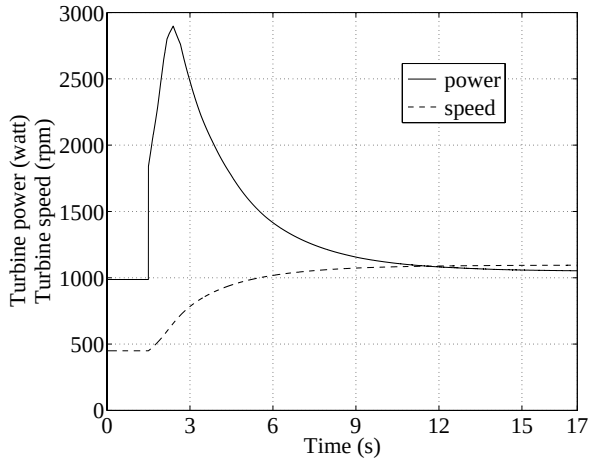

Fig. 16 Captured power of wind turbine and turbine speed for SOC = 0.3, G changed suddenly from 0.1 kW/m^2 to 1 kW/m^2 at t = 1.5 s and V_w changed suddenly from 10.5 m/s to 15 m/s at t = 1.5 s.

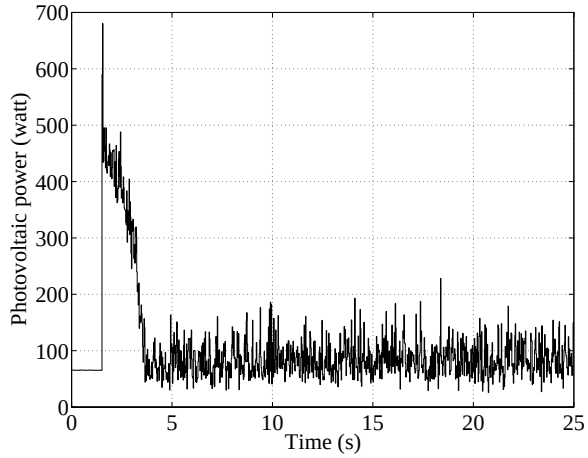

Fig. 19 Captured power of PV array for SOC = 0.9, G changed suddenly from 0.1 kW/m^2 to 1 kW/m^2 at t = 1.5 s and V_w changed suddenly from 4 m/s to 10.5 m/s at t = 1.5 s.

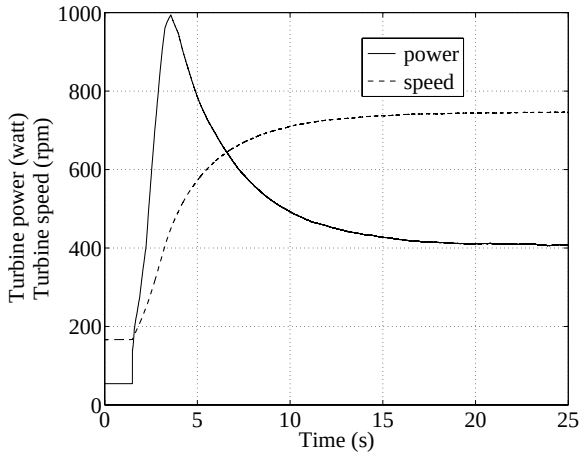

Fig. 20 Captured power of wind turbine and turbine speed for SOC = 0.9, G changed suddenly from 0.1 kW/m^2 to 1 kW/m^2 at t = 1.5 s and V_w changed suddenly from 4 m/s to 10.5 m/s at t = 1.5 s.

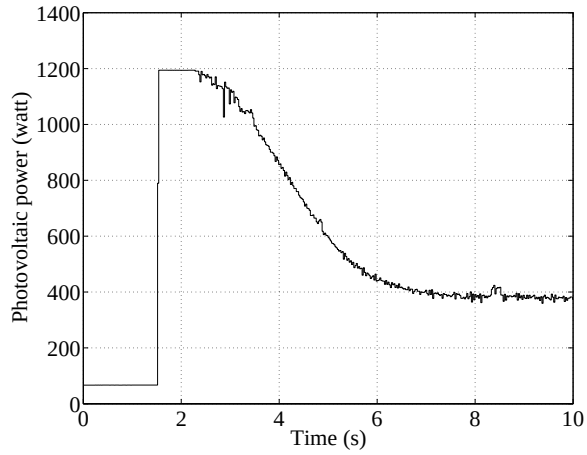

Fig. 23 Captured power of PV array for SOC = 0.9, R_L = 20 Ω, G changed suddenly from 0.1 kW/m^2 to 1 kW/m^2 at t = 1.5 s and V_w changed suddenly from 4 m/s to 10.5 m/s at t =1.5 s.

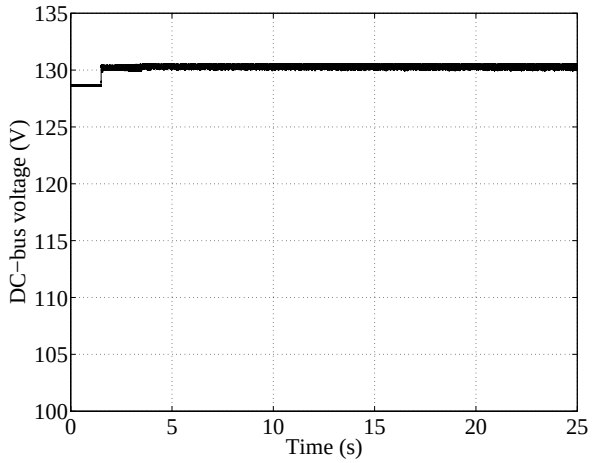

Fig. 21 DC-bus voltage for SOC = 0.9, G changed suddenly from 0.1 kW/m^2 to 1 kW/m^2 at t = 1.5 s and V_w changed suddenly from 4 m/s to 10.5 m/s at t = 1.5 s.

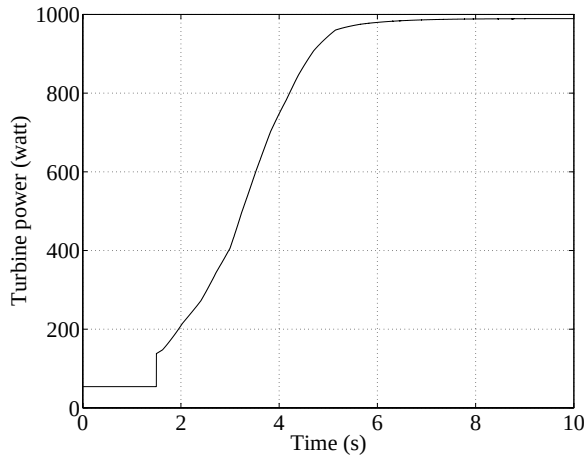

Fig. 24 Captured power of wind turbine for SOC = 0.9, R_L = 20 Ω, G changed suddenly from 0.1 kW/m^2 to 1 kW/m^2 at t = 1.5 s and V_w changed suddenly from 4 m/s to 10.5 m/s at t =1.5 s.

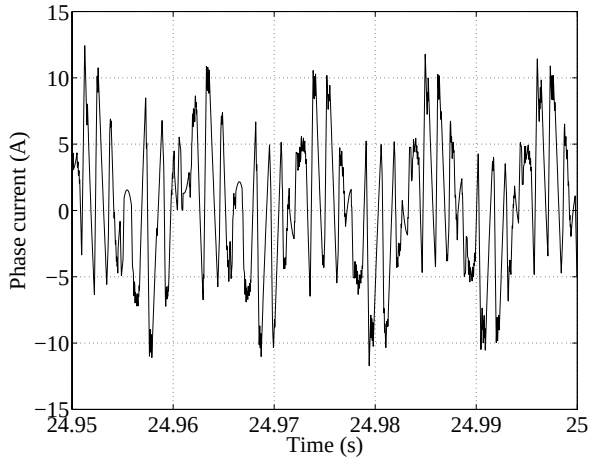

Fig. 22 Steady-state phase current of the induction generator for SOC = 0.9, G changed suddenly from 0.1 kW/m^2 to 1 kW/m^2 at t = 1.5 s and V_w changed suddenly from 4 m/s to 10.5 m/s at t = 1.5 s.

CONCLUSION

Performance of stand-alone hybrid wind-PV system with battery storage is studied. The proposed wind subsystem using SCIG and DTC technique is studied. The reactive power required by SCIG is obtained from the battery bank through PWM rectifier. According to the battery-bank voltage (u_{dc}), there are two modes of operation of the system. One mode when the battery-bank voltage is less than or equal to the maximum voltage limit, and the other mode when the battery-bank voltage exceeds the maximum voltage limit. In the first mode, the battery-bank voltage is below its maximum value, and thus the PV and wind subsystems are allowed to follow their maximum powers. In the second mode, the captured power is limited such that the battery bank voltage does not exceed its maximum value. Modeling and control of the system are demonstrated. Good performance of the system is verified by the results obtained for each mode of operation.

REFERENCES

[1] L.-Q. Liu and Z.-X. Wang, "The development and application practice of wind-solar energy hybrid generation systems in China," Renewable and Sustainable Energy Reviews, no. 13, pp. 1504─1512, 2009.

[2] F. Valenciaga and P. F. Puleston, "Supervisor control for a stand-alone hybrid generation system using wind and photovoltaic energy," IEEE Trans. Energy Conversion, vol. 20, no. 2, pp. 398─405, June 2005.

[3] S. A. Daniel and N. AmmasaiGounden, "A novel hybrid isolated generating system based on PV fed inverter-assisted wind-driven induction generators," IEEE Trans. Energy Conversion, vol. 19, no. 2, pp. 416─422, June 2004.

[4] B. S. Borowy and Z. M. Salameh, "Methodology for optimally sizing the combination of a battery bank and PV array in a wind/PV hybrid system," IEEE Trans. Energy Conversion, vol. 11, no. 2, pp. 367─375, June 1996.

[5] F. Valenciaga and P. F. Puleston, "High-order sliding control for a wind energy conversion system based on a permanent magnet synchronous generator," IEEE Trans. Energy Conversion, vol. 23, no. 3, pp. 860─867, Sep. 2008.

[6] B. S. Borowy and Z. M. Salameh, "Dynamic response of a stand-alone wind energy conversion system with battery energy storage to a wind gust," IEEE Trans. Energy Conversion, vol. 12, no. 1, pp. 73─78, March 1997.

[7] E. Koutroulis and K. Kalaitzakis, "Design of a maximum power tracking system for wind-energy-conversion applications," IEEE Trans. Ind. Electron., vol. 53, no. 2, pp. 486─494, April 2006.

[8] M. H. Nehrir, B. J. LaMeres, G. Venkataramanan, V. Gerez, and L. A. Alvarado, "An approach to evaluate the general performance of stand-alone wind/photovoltaic generating systems," IEEE Trans. Energy Conversion, vol. 15, no. 4, pp. 433─439, Dec. 2000.

[9] J. P. Dunlop, "Batteries and charge control in stand-alone photovoltaic systems, fundamentals and application," Report, Sandia National Laboratories, Photovoltaic systems Applications Dept., Jan. 1997.

[10] K. K. Tse, B. M. T. Ho, H. S.-H. Chung, and S. Y. R. Hui, "A comparative study of maximum-power-point trackers for photovoltaic panels using switching-frequency modulation scheme," IEEE Trans. Ind. Electron., vol. 51, no. 2, pp. 410─418, April 2004.

[11] T. Markvart, "Solar electricity," Book, John Wiley & Sons, 1995.

[12] J. H. R. Enslin, M. S. Wolf, D. B. Snyman, and W. Swiegers, " Integrated photovoltaic maximum power point tracking converter," IEEE Trans. Ind. Electron., vol. 44, no. 6, pp. 769─773, Dec. 1997.

[13] Y.-H. Kim and H.-D. Ha, "Design of interface circuits with electrical battery models," IEEE Trans. Ind. Electron., vol. 44, no. 1, pp. 81─86, Feb. 1997.

[14] Z. M. Salameh, M. A. Casacca, and W. A. Lynch, "A mathematical model for lead-acid batteries," IEEE Trans. Energy Conversion, vol. 7, no. 1, pp. 93─98, March 1992.

[15] E. Koutroulis, K. Kalaitzakis, and N. C. Voulgaris, "Development of a microcontroller- based, photovoltaic maximum power point tracking control system," IEEE Trans. Power Electron., vol. 16, no. 1, pp. 46─54, Jan. 2001.

[16] A. M. De Broe, S. Drouilhet, and V. Gevorgian, "A peak power tracker for small wind turbines in battery charging applications," IEEE Trans. Energy Conversion, vol. 14, no. 4, pp. 1630─1635, Dec. 1999.

[17] M. R. Patel, "Wind and solar power systems," Book, CRC Press, 1999.

[18] D. S. Zinger and E. Muljadi, "Annualized wind energy improvement using variable speeds," IEEE Trans. Ind. Applicat., vol. 33, no. 6, pp. 1444─1447, Nov./Dec. 1997.

[19] R. Karki and R. Billinton, "Reliability/cost implication of PV and wind energy utilization in small isolated power systems," IEEE Trans. Energy Conversion, vol. 16, no. 4, pp. 368─373, Dec. 2001.

[20] O. E. S. Mohammed, N. M. B. Abdel-Rahim, and A. Shaltout, "Stand-alone wind system with battery storage using induction generator and direct torque control," 13th Middle East Power Systems Conference, MEPCON' 2009, Egypt, pp. 50─56, Dec. 2009.

[21] SIMULINK 7, The MathWorks, Inc., 2007.

[22] R. Perez, "Lead-acid battery state of charge vs. voltage," Home Power, no. 36, pp. 66─69, Aug./Sep. 1993.

APPENDIX I

A. *Data of PV array*

The PV array is arranged in two strings, and each string consists of five series modules. The PV module has the following specifications:

Maximum power = 120 watt, voltage at maximum power = 16.9 V, current at maximum power = 7.1 A, open-circuit voltage = 21 V, short-circuit current = 7.7 A, and the current–Voltage characteristics of the PV module at different insolation levels and cell temperature of 25° C are shown in Fig. 25.

B. *Data of Wind Turbine and Induction generator*

Wind turbine has the following data:

C_p-α characteristics shown in Fig. 4,

Rated power = 0.994 kW, rotor blade = 1.1 m,

$V_{cut\text{-}in}$ = 4 m/s, V_{rated} = 10.5 m/s and $V_{cut\text{-}out}$ = 20 m/s

The induction generator is: Δ-connected, 1.1 kW, $110/\sqrt{3}$ V, 12.45 A, 3386 rpm, 2 poles, 60 Hz, and has the following parameters: R_s = 0.515 Ω, R_r = 0.517, L_{ls} = 1.6 mH, L_{lr} = 1.6 mH and L_m = 0.0701 H.

Total inertia of wind turbine and induction generator (referred to turbine side) = 1 kg.m^2, gear ratio = 7.38.

C. *Data of DC-DC converter*

Step-up converter of the following data: of Inductance = 1.1 mH, capacitance = 10 mF and switching frequency = 25 kHz.

D. *Data of PWM rectifier*

Rectifier states are reviewed every 33 μsec. This means that each of the turn-on and turn-off times of the rectifier switches has minimum value of 33 μsec and, hence, the maximum switching frequency is about 15.15 kHz.

E. *Data of battery bank*

The battery-bank voltage used in this paper is 120 V. The battery bank consists of ten batteries. Each battery is 12 V, 175 Ah deep-cycle, lead-acid battery, and has characteristics derived from measured data [22]. The derived characteristics are given in TABLE I. The maximum voltage limit of one battery is U_{boc} at SOC = 1 which is equal to 13.039 V.

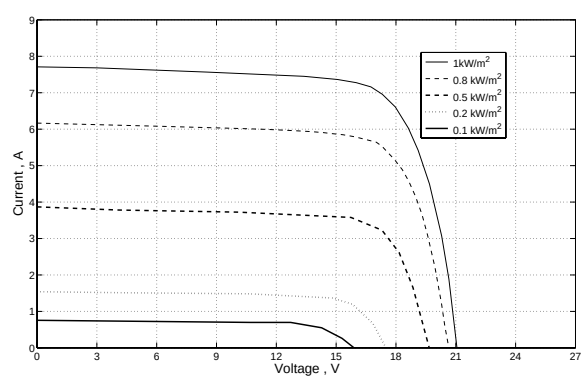

Fig. 25 PV module characteristics at different insolation levels.

TABLE I
BATTERY PARAMETERS

Equivalent circuit parameters	State of charge (SOC)	
	0.3	0.9
U_{boc} (V)	12.401	12.804
R_c (Ω)	0.0172	0.0712
R_d (Ω)	0.0304	0.0174